SCIENCE CHINA
Technological Sciences

• Article •

December 2015 Vol.58 No.12: 2195–2206
doi: 10.1007/s11431-015-5962-5

Acquisition algorithm assisted by AGC control voltage for DSSS signals

SHEN YuYao, WANG YongQing*, LIU MinLi & WU SiLiang

School of Information and Electronics, Beijing Institute of Technology, Beijing 100081, China

Received September 9, 2015; accepted October 26, 2015

An appropriate acquisition configuration in terms of signal quality can optimize the acquisition performance. In view of this, a new approach of acquisition assisted by the control voltage of automatic gain control (AGC) is proposed. This approach judges the signal power according to the AGC control voltage and switches the working modes correspondingly and adaptively. Non-coherent accumulation times and the detection threshold are reconfigured according to the working mode. Theoretical derivation and verification by simulation in typical situations are provided, and the algorithm is shown to be superior in terms of the mean acquisition time, especially in strong signal scenarios compared with the conventional algorithm.

direct sequence spread spectrum, acquisition, AGC control voltage, carrier-to-noise density ratio estimation, adaptive working mode switch

Citation: Shen Y Y, Wang Y Q, Liu M L, et al. Acquisition algorithm assisted by AGC control voltage for DSSS signals. Sci China Tech Sci, 2015, 58: 2195–2206, doi: 10.1007/s11431-015-5962-5

1 Introduction

The direct sequence spread spectrum (DSSS) plays an important role in the fields of telemetry, tracking and command (TT&C), global navigation satellite system (GNSS) [1], civil communication [2–4], and so on, due to its strong anti-jamming capacity and superior anti-interception performance [5,6]. The acquisition unit is crucial to the synchronization of a DSSS signal [7], in which signal detection is performed and coarse synchronization of Doppler frequency and code phase are obtained by acquisition. Subsequently, the tracking unit begins operation on the basis of the coarse synchronization results to realize a finer synchronization [8,9]. In addition to the detection and false-alarm probabilities (called detection performance hereafter) [10,11] and the computation load [12], the mean acquisition time (MAT) is an important figure of merit in evaluating the detection performance, i.e., performance of the acquisition process. Some studies aimed at fast implementation methods based on alternative transformations or elimination of operation redundancies [13,14], whereas others stressed on designing of acquisition algorithms [15–17]. This paper has the latter focus.

The design of an acquisition algorithm depends on the quality of the received signal. In practice, fluctuation in the carrier-to-noise density ratio (CNR) of a received signal spans a wide range because of the variance of the transmit channel properties and the distance between the transmitter and the receiver. As a result, the optimal configuration of an acquisition unit in terms of reducing MAT is never constant [15]. The conventional acquisition algorithm ignores this aspect and typically equipped with a fixed predetermined configuration corresponding to a particular CNR, which is generally the lower bound of CNR uncertainty range [18]. This configuration will result in MAT performance degradation when other potential CNR situations beyond the de-

*Corresponding author (email: wangyongqing@bit.edu.cn)

sign CNR are encountered. Therefore, it is of practical importance to study algorithms for signal detection that are robust against the commonly encountered uncertainties and that can work reliably at various practical CNRs. In view of this, a large number of related acquisition algorithms have been developed, most of which work on the basis of CNR estimation of received signal [16,17] and regulation of parameters, such as the selection of detection threshold [17] and correlation time [19].

As described in the preceding text, acquisition configuration relies on the CNR of the received signal. For a DSSS system, CNR estimators generally rely on the post-correlation value of the signal power in their calculations. Some of these CNR estimators operate after the signal has already been synchronized [16]; therefore, although they have high precision, they are not useful for acquisition configuration because acquisition has already been completed. Other estimators operate during the maximum likelihood search in a two-dimensional uncertainty region. These estimators are based on two-dimensional correlation results. In view of this, to adjust the acquisition configuration, an additional prior correlation is needed before conventional acquisition. As noted in ref. [17], in the threshold generation mode, where the additional prior correlation is carried out, the correlation result as a measure of the merit of CNR estimation is used as a reference to adjust the thresholds in the following search and verification mode. This method performs well in low CNR scenarios, because the optimized threshold greatly reduces the time cost of search mode, which not only compensates for the additional time spent on the prior correlation but also reduces the total time consumption. In contrast, in high CNR situations, the time cost of search mode is commensurate with the additional correlation time, and the time saving from threshold optimization cannot compensate for the additional time cost of the prior correlation. Therefore, additional prior correlation results in MAT performance degradation. Some studies focused directly on the optimization of acquisition configuration, with on attention paid to CNR estimation. For example, an enhanced acquisition algorithm equipped with a Tong detector was proposed in ref. [19]. To decrease MAT, the algorithm places emphasis on optimization of non-coherent accumulation times, along with adaptation of parameters of the Tong detector. The mentioned optimization is based on a priori knowledge of signal-to-noise ratio (SNR), which is the product of CNR and signal bandwidth. Usually, this type of algorithms have to rely on assistance from outside professional equipment with the CNR estimation function. Such dependency incurs great limitations on their applications.

Automatic gain control (AGC) is widely used in DSSS receivers. Its control voltage can reflect the power of received signal and work as a metric for signal quality. In the previous research, AGC as an interference assessment and detection tool [20–22] has been already presented. Similarly, for near-field TT&C responders and navigation receivers, where the target signal is still of large power in the receiver end, AGC can also possibly work as a desired signal assessment tool and offer assistance information for acquisition configuration, although to the authors' knowledge, related research is not available in the published literatures.

In view of this, an acquisition algorithm assisted by AGC control voltage is proposed in this paper; the algorithm judges the signal power according to the AGC control voltage and performs an adaptive working mode switch correspondingly, in order to accelerate the acquisition process. The correlation time and detection threshold are configured for each working mode to improve the MAT performance. Even though the proposed algorithm has limited sensitivity to mode switching when CNR is low, it performs well in high CNR situations because the AGC control voltage is more effective in this region. Therefore, combining the proposed algorithm and the algorithm proposed in ref. [17] can achieve a better performance in both low CNR and high CNR scenarios. In addition, as AGC is applied to most receivers, the proposed algorithm will not noticeably increase consumption of the hardware resources or power dissipation compared with the algorithms based on the CNR estimation utilizing post-correlation results. Therefore, the proposed algorithm is extremely suitable for applications such as space-borne facilities where it is necessary to reduce MAT without an increase in hardware costs because of the restrictions on power dissipation and receiver size.

The remainder of this paper is organized as follows. Section 2 describes the principles of AGC and conventional acquisition. Section 3 introduces the acquisition algorithm assisted by AGC control voltage. In Section 4, expressions for the detection performance, MAT, and computational complexity of the proposed algorithm are derived. Simulation results of the proposed algorithm are presented in Section 5, along with comparisons with the conventional algorithm. Some conclusions are drawn in Section 6.

2 Principles of AGC and conventional acquisition

2.1 Principles of AGC

Owing to the large dynamic range of working distance, onboard spread spectrum equipment, such as TT&C responders and navigation receivers, have a large dynamic range of input signal power, which generally exceeds 70 dB [23]. In addition, rapid movement of aircraft (>10 km/s) results in continuous fluctuation of the input signal power. Therefore, AGC is important for onboard equipment to ensure a sufficient dynamic range of input baseband signals.

Figure 1 shows a block diagram of AGC. A signal power detector and variable gain amplifier (VGA) are essential parts of AGC. The former is responsible for signal power monitoring, as its name implies, and also outputs a control voltage V_{GAIN} as an indicator of received signal strength. VGA is responsible for the regulation of input signal power

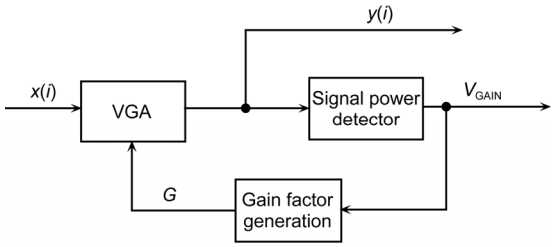

Figure 1 Block diagram of AGC.

under the control of the gain factor derived from the control voltage. In Figure 1, G denotes the gain factor mentioned above, $x(i)$ and $y(i)$ denote the input and output signal sequences of the AGC module, respectively.

2.2 Principles of conventional acquisition

For digital baseband DSSS signal acquisition, the received signal can be represented as [24]

$$s[n]=\sqrt{P_s}b\left[nT_s-\tau\right]c\left[nT_s-\tau\right]\exp\left[j\left(2\pi f_d nT_s+\theta\right)\right]+w\left[n\right], \tag{1}$$

where P_s is the power of desired signal. $b[nT_s-\tau]$ and $c[nT_s-\tau]$ denote the data-bit samples and pseudo random code sequence, respectively, wherein τ is the code delay and T_s is the interval of sample time. f_d is the frequency offset, mainly the Doppler frequency. θ is the carrier phase offset. The noise sequence denoted as $w[n]$ is complex Gaussian distributed, which can be expressed as $w[n]\sim\mathcal{CN}(0,\sigma^2)$.

The decision variable Λ is obtained by accumulating the square modulus of coherent integration results, i.e.,

$$\Lambda=\sum_{m=0}^{M-1}\left|r\left[m\right]\right|^2, \tag{2}$$

where $r[m]$ is the coherent integration result and M denotes the non-coherent accumulation times. The statistic of Λ is central Chi-square distributed with $2M$ degrees of freedom under hypothesis H_0; otherwise, under hypothesis H_1, Λ is non-central Chi-square distributed with the same degrees of freedom [25]. Here, H_0 and H_1 represent the null and alternative hypotheses, respectively. The expressions for the false-alarm and detection probabilities on the cell level are

$$p_{fa}\left(M,\gamma\right)=\exp\left(-\frac{\gamma}{2\sigma_n^2}\right)\sum_{m=0}^{M-1}\frac{1}{m!}\left(\frac{\gamma}{2\sigma_n^2}\right)^m, \tag{3}$$

$$p_d\left(M,\gamma\right)=Q_M\left(\sqrt{2M\eta_c},\sqrt{\gamma/\sigma_n^2}\right), \tag{4}$$

where γ denotes the detection threshold, σ_n^2 is the noise variance after coherent integration, η_c is the non-centrality parameter that represents the SNR of coherent integration results, and $Q_M(a,b)$ is the generalized Marcum-Q function [25].

3 Principles of AGC and conventional acquisition

Firstly the architecture of AGC control voltage assisting the acquisition algorithm is presented in this section. Subsequently, the mutual relationship between AGC control voltage and CNR of the input signal, which lays the foundation of the proposed algorithm, is analyzed in the form of equations. Finally, the law of mode switching according to CNR estimation obtained from the AGC control voltage is described in detail.

3.1 Architecture of proposed algorithm

As mentioned before, because AGC control voltage is an indicator of CNR, it would be helpful for the design of acquisition unit to consider the correlation time and the detection threshold. Figure 2 shows a detailed block diagram of the proposed algorithm.

As shown in this figure, the proposed algorithm can be divided into four parts, namely, AGC module, CNR estimation module, mode switching module, and conventional acquisition unit, whose functions are as follows.

a) The AGC module monitors the received signal power and provides a control voltage to the CNR estimation module. It also adjusts the signal power to an appropriate level for the following acquisition, tracking, and so on.

b) The CNR estimation module makes use of the AGC control voltage to calculate the CNR of the received signal. It works as a bridge between the AGC control voltage and the mode switch, and can be pre-calculated instead of attending the implementing in a field-programmable gate array (FPGA).

c) The mode switching module performs the mode switching according to the CNR estimation. Using this module, the parameters of non-coherent accumulation times M and detection threshold are configured and delivered to the corresponding modules.

d) The conventional acquisition unit performs acquisition, by exploiting the AGC adjusted signals with the configuration provided by the mode switching module.

The conventional acquisition unit is the same as that in previous research [26], and will not be described in the following sections. Similarly, the AGC module is not described because it has also become a well-established product [27]. The other two parts of the proposed algorithm, which are highlighted with gray in the block diagram, will be introduced in detail.

3.2 CNR estimation

In the AGC unit, the relationship between the received signal

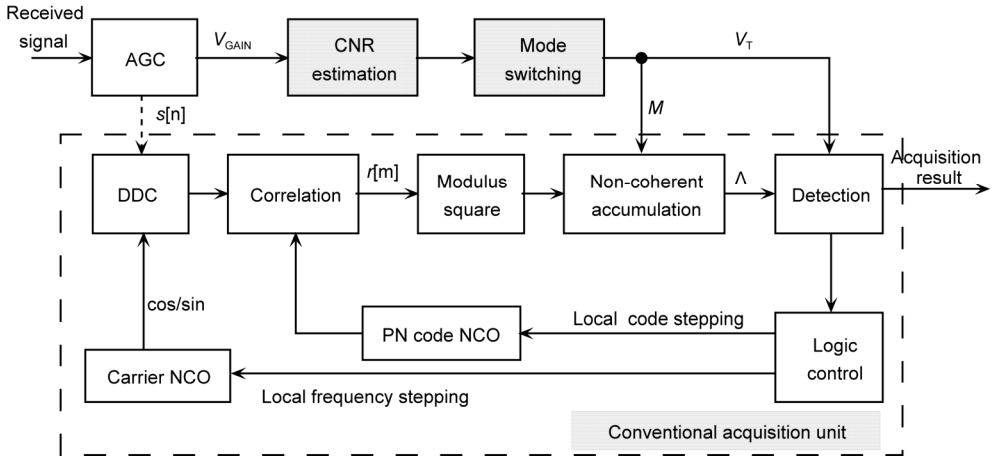

Figure 2 Block diagram of proposed acquisition algorithm assisted by AGC control voltage.

power P and the control voltage V_{GAIN} can be expressed as

$$V_{GAIN} = f(P), \tag{5}$$

where P is the summation of noise power P_n and desired signal power P_s, ignoring other interferences, i.e.,

$$P = P_s + P_n = \left(10^{\eta/10} + 1\right) P_n, \tag{6}$$

where the input SNR in dB, denoted as η, is defined as

$$\eta = 10\log_{10}\left(P_s / P_n\right). \tag{7}$$

The specific definition of the function f is provided by the datasheet of the AGC device. Clearly, the received signal power P serves as a link connecting V_{GAIN} and η. Therefore, η and V_{GAIN} can be derived from each other, i.e.,

$$\begin{cases} \eta = 10\log 10\left[\dfrac{f^{-1}\left(V_{GAIN}\right) - P_n}{P_n}\right], \\ V_{GAIN} = f\left(10^{\eta/10} P_n + P_n\right). \end{cases} \tag{8}$$

In practice, P_n can be evaluated because the configuration of receiver front-end is completely known and the fluctuation of noise power is tolerable at extremely high SNRs. In this theoretical analysis, for simplicity, only basic noise is considered, and the noise introduced by the front-end of the receiver is ignored. This simplification will not interfere with the expression of the essential thought of the proposed algorithm. Thus, the noise power in dBw is

$$P_n\ (\text{dBw}) = 10\log_{10}\left(\mathcal{K}TB\right), \tag{9}$$

where the Boltzmann constant denoted as $\mathcal{K}$ is 1.38×10^{-23} J/K. The kelvin temperature T is typically 293 K. B, which represents the bandwidth of the DSSS signal is equals to approximately $2R_c$, where R_c is the code rate. Taking the C/A signal in the GPS system as an example, which has a code length of 1023 chips and a code rate of 1.023 Mcps [8], the noise power is approximately −141dBw, i.e., $10\log_{10}(1.38\times10^{-23}\times293\times2.046\times10^{6})$.

If η is relatively small, P_n plays an extremely dominant role in P, and as a result V_{GAIN} is insensitive and can hardly reflect the CNR variation accurately. Therefore, there is a lower bound of η at which a reliable η can be derived from V_{GAIN}. This lower bound of η is denoted as η_0. Then the corresponding CNR bound ρ_0 is

$$\rho_0 = \eta_0 + 10\log_{10} B = \eta_0 + 10\log_{10} f_c + 3. \tag{10}$$

Experientially, estimation of η is reliable if P_n contributes less than 90 percent of P. Therefore, η_0 is approximately −10 dB, and the corresponding ρ_0 is $-7+10\log_{10}f_c$.

Numerical results of a specific AGC device, i.e., AD8367, are presented in the Appendix A as an intuitive interpretation.

3.3 Mode switching

Mode switching realizes adaptive accommodation of acquisition configuration to various CNRs. Prolonging the coherent integration time T_{coh} is not an ideal option for improving the detection performance because of the presence of unknown data-bits and residual frequency offset [24]. Therefore, only M and γ remain as the parameters of interest for achieving the desired detection performance. The configuration of M and γ are the kernel of mode switching: a large M ensures detection performance; however, if CNR is sufficiently high to meet the demand of detection performance merely with a single-code-period coherent integration, a large M value is unnecessary and brings negative effects on the MAT performance. Therefore, to accelerate the acquisition process, M should be minimized on the premise that the desired detection performance is achieved.

Generally, for a desired detection performance of a certain acquisition algorithm, the lower bound of detection SNR in dB, denoted as η_{th}, can be obtained, and the corre-

sponding CNR bound ρ_{th} is

$$\rho_{th} = \eta_{th} - 10\log_{10} T_{coh} - G(M), \tag{11}$$

where $G(M)$ represents the SNR improvement caused by M times non-coherent accumulation, and $G(M) \geqslant G(1) = 0$. Combining (10) and (11) gives

$$\begin{aligned}\rho_0 - \rho_{th} &= \eta_0 + 10\log_{10} f_c + 3 - \eta_{th} + 10\log_{10} T_{coh} + G(M) \\ &\geqslant \eta_0 - \eta_{th} + 10\log_{10} L + 3,\end{aligned} \tag{12}$$

where $L=f_cT_{coh}$ expresses the code length. Eq. (12) shows that the minimum CNR interval between ρ_0 derived from AGC control voltage and ρ_{th} is mainly determined by L. The empirical value of η_{th} is less than 16 dB with signal dwell detection. Therefore, when $L\geqslant 255$, which is in line with the general TT&C and GNSS applications, $\rho_0-\rho_{th}$ is positive. This means that the AGC control voltage merely indicates the situations where CNR is sufficiently high to achieve the desired detection performance by acquisition configuration with M=1. Furthermore, in such situations, both the acquisition complexity and MAT are reduced compared with the conventional algorithm.

Let us assume that M_L is the optimal value of M corresponding to the lower bound of potential CNR in practice, which is also the constant configuration of conventional algorithm. Without loss of generality, f is assumed as an increasing function. Then, M of the proposed algorithm is M_L if $V_{GAIN}<V_t$, and 1 otherwise. V_t is the threshold of AGC control voltage corresponding to ρ_0, i.e.,

$$V_t = g(\rho_0) = f\left(10^{(\rho_0 + 10\log_{10} T_c - 3)/10} P_n + P_n\right). \tag{13}$$

In conclusion, with the assistance of AGC control voltage, the proposed algorithm can be divided directly into two working modes: a) when $V_{GAIN} \geqslant g(\rho_0)$ (i.e., in the higher CNR mode), the simplest scheme with M=1 and the corresponding $\gamma=\gamma_1$ is utilized in the acquisition unit; and b) when $V_{GAIN} < g(\rho_0)$ (i.e., in the lower CNR mode), the scheme with $M=M_L$ and $\gamma=\gamma_L$ is utilized, which is the same as the conventional algorithm. γ is obtained at a constant false-alarm rate and can be derived according to (14). When $M \neq 1$, the closed form of γ is difficult to obtain; therefore, a numerical approach is preferred.

4 Performance analysis

In this section, the performance of the proposed algorithm is analyzed and a comparison between the proposed and the conventional algorithms is drawn. The analyses are performed in three aspects: detection performance, MAT performance, and computational complexity.

4.1 Detection performance

Detection performance, namely the detection and false-alarm probabilities at certain CNRs, is evaluated by mathematical formulas in this subsection. The derivation is developed under three well-known search strategies: parallel, serial, and hybrid search.

The detection performance of a parallel acquisition algorithm is investigated at first. Let us assume that the number of search bins involved in the two-dimensional uncertainty region is N; then the expressions of the false-alarm and detection probabilities on the system level are

$$P_{FA}^{(p)}(\gamma) = 1 - \left[1 - P_{fa}(M,\gamma)\right]^N = \begin{cases} 1 - \left[1 - \exp\left(-\dfrac{\gamma}{2\sigma_n^2}\right)\displaystyle\sum_{m=0}^{M_L-1}\frac{1}{m!}\left(\frac{\gamma}{2\sigma_n^2}\right)^m\right]^N, \\ \qquad\qquad V_{GAIN} < g(\rho_0), \\ 1 - \left[1 - \exp\left(-\dfrac{\gamma}{2\sigma_n^2}\right)\right]^N, \quad V_{GAIN} \geqslant g(\rho_0), \end{cases} \tag{14}$$

$$P_D^{(p)} = \begin{cases} \displaystyle\int_{\gamma_L}^{\infty} f_{H_1}(M_L, x)\left[1 - P_{fa}(M_L, x)\right]^{N-1}\mathrm{d}x, \\ \qquad\qquad V_{GAIN} < g(\rho_0), \\ \displaystyle\int_{\gamma_1}^{\infty} f_{H_1}(1, x)\left[1 - P_{fa}(1, x)\right]^{N-1}\mathrm{d}x, \\ \qquad\qquad V_{GAIN} \geqslant g(\rho_0), \end{cases} \tag{15}$$

where $f_{H_1}(M,x)$ is the probability density function of decision variable Λ in the H_1 bin, which can be expressed as

$$f_{H_1}(M,x) = \frac{1}{2\sigma_n^2}\left[\frac{x}{2\sigma_n^2 M\eta_c}\right]^{M-1} \mathrm{I}_{M-1}\left(\sqrt{\frac{2M\eta_c x}{\sigma_n^2}}\right) \times \exp\left[-\left(\frac{x}{2\sigma_n^2} + M\eta_c\right)\right], \tag{16}$$

where $\mathrm{I}_v(\cdot)$ is the vth-order modified Bessel function of the first kind [28]. In brief, compared with the conventional algorithm [29], the main difference in the detection performance occurs in the condition that $V_{GAIN} \geqslant g(\rho_0)$.

The false-alarm probabilities of both serial and hybrid search strategies are the same as that of the parallel strategy. Their detection probabilities can be derived respectively as

$$P_D^{(s)} = \frac{1 - \left[1 - P_{fa}(M,\gamma)\right]^N}{P_{fa}(M,\gamma)} \int_{\gamma}^{\infty} f_{H_1}(M,x)\mathrm{d}x, \tag{17}$$

and

$$P_D^{(h)} = \frac{C_p}{N}\frac{1 - \left[1 - P_{fa}(M,\gamma)\right]^N}{1 - \left[1 - P_{fa}(M,\gamma)\right]^{C_P}} \times \int_{\gamma}^{\infty}\left[1 - P_{fa}(M,\gamma)\right]^{C_p - 1} f_{H_1}(M,x)\mathrm{d}x, \tag{18}$$

where $M=M_L$ and $\gamma=\gamma_L$ if $V_{GAIN} < g(\rho_0)$; otherwise $M=1$ and $\gamma=\gamma_1$. C_p is the number of parallel correlators, $P_D^{(s)}$ and $P_D^{(h)}$ denote the detection probabilities of serial search and hybrid search, respectively.

Clearly, at low CNRs, the proposed algorithm has identical detection performance to the conventional algorithm [29]. At high CNRs, the detection performance of the proposed algorithm is slightly degraded but still very close to the performance of the conventional algorithm which will be verified by numerical results in Section 5.

4.2 MAT performance

As a common metric used to assess the performance of acquisition units, MAT is evaluated in this section. The three strategies mentioned in Subsection 4.1 are also considered.

First, taking parallel search strategy into consideration, the MAT of the proposed algorithm is exactly the observation length MT_{coh} [30]. MAT is clearly directly proportional to the non-coherent times.

The MATs of the other two search strategies have a similar tendency to the MAT of parallel search. The expressions of MAT for serial search strategy and hybrid search strategy, denoted as $T_{pro}^{(s)}$ and $T_{pro}^{(h)}$, respectively, can be written as

$$T_{pro}^{(s)} = \begin{cases} \dfrac{2+\left[2-P_d\left(M_L,\gamma_L\right)\right]\left(N-1\right)\left[1+K_P P_{fa}\left(M_L,\gamma_L\right)\right]}{2P_d\left(M_L,\gamma_L\right)} M_L T_{coh}, \\ \qquad\qquad V_{GAIN} < g\left(\rho_0\right), \\ \dfrac{2+\left[2-P_d\left(1,\gamma_1\right)\right]\left(N-1\right)\left[1+K_P P_{fa}\left(1,\gamma_1\right)\right]}{2P_d\left(1,\gamma_1\right)} T_{coh}, \\ \qquad\qquad V_{GAIN} \geqslant g\left(\rho_0\right), \end{cases} \tag{19}$$

and

$$T_{pro}^{(h)} = \begin{cases} \dfrac{2+\left[2-P_d^{(h)}\left(M_L,\gamma_L\right)\right]\left(\dfrac{N}{C_p}-1\right)\left[K_P P_{fa}^{(h)}\left(M_L,\gamma_L\right)+1\right]}{2P_d^{(h)}\left(M_L,\gamma_L\right)} M_L T_{coh}, \\ \qquad\qquad V_{GAIN} < g\left(\rho_0\right), \\ \dfrac{2+\left[2-P_d^{(h)}\left(1,\gamma_1\right)\right]\left(\dfrac{N}{C_p}-1\right)\left[K_P P_{fa}^{(h)}\left(1,\gamma_1\right)+1\right]}{2P_d^{(h)}\left(1,\gamma_1\right)} T_{coh}, \\ \qquad\qquad V_{GAIN} \geqslant g\left(\rho_0\right), \end{cases} \tag{20}$$

where K_p, called the penalty factor [31], is the ratio between time consumption due to false alarm and the single dwell time of acquisition. $P_d^{(h)}(M,\gamma)$ is the detection probability of parallel search block containing the H_1 bin and $P_{fa}^{(h)}(M,\gamma)$ is the false-alarm probability of parallel search blocks containing H_0 bins only. The corresponding expressions are

$$\begin{cases} P_d^{(h)}\left(M,\gamma\right) = \displaystyle\int_{\gamma}^{\infty}\left[1-P_{fa}\left(M,x\right)\right]^{C_p-1} f_{H_1}\left(M,x\right)\mathrm{d}x, \\ P_{fa}^{(h)}\left(M,\gamma\right) = 1-\left[1-P_{fa}\left(M,\gamma\right)\right]^{C_p-1}. \end{cases} \tag{21}$$

As mentioned before, the detection performance of the proposed algorithm is very close to the conventional one, i.e., $P_d(1,\gamma_1) \approx P_d(M_L,\gamma_L)$ and $P_{fa}(1,\gamma_1) = P_{fa}(M_L,\gamma_L)$, when $V_{GAIN} \geqslant g(\rho_0)$. Therefore, in the lower and normal CNR conditions, the proposed algorithm has an equal performance in terms of MAT compared with the conventional algorithm [30] with all of the three search strategies, whereas in high CNR conditions where the AGC power metric contributes to the acquisition parameter set, the proposed algorithm performs better by M times in terms of MAT.

4.3 Computational complexity and resource utilization

To fully compare the performance of different acquisition algorithms, computational load should be considered. Therefore, in this subsection the conventional and proposed algorithms are briefly analyzed in terms of computational complexity. Because the circular correlation based on fast Fourier transform (FFT) is extensively used, it is taken as an example here to illustrate the computational complexity performance. The computational loads are listed in Table 1, where N_s represents the number of samples within the duration of a single coherent integration and N_c and N_{fd} represent the number of bins in the code phase domain and that in the Doppler frequency domain respectively.

According to the bottom row in the table, the numbers of multiplication and summation, denoted as Π_{mult} and Π_{sum}, can be further summarized as

Table 1 Computational loads

Module	Multiplication	Summation
DDC	$4MN_{fd}N_s$	$2MN_{fd}N_s$
FFT-based correlation	MN_{fd} [$6N_s\log_2(N_s)+4N_s$]	MN_{fd} [$9N_s\log_2(N_s)+2N_s$]
Square modulus	$2MN_{fd}N_c$	$MN_{fd}N_c$
Non-coherent accumulation	0	(M-1) $N_{fd}N_c$
Maximum choosing & decision	0	$N_{fd}N_c$
Total	MN_{fd} [$8N_s+6N_s\log_2(N_s)+2N_c$]	MN_{fd} [$4N_s+9N_s\log_2(N_s)+(1+1/M)N_c$]

$$\Pi_{mult}=\begin{cases}M_L N_{fd}\left[8N_s+6N_s\log_2\left(N_s\right)+2N_c\right], & V_{GAIN}<g\left(\rho_0\right),\\ N_{fd}\left[8N_s+6N_s\log_2\left(N_s\right)+2N_c\right], & V_{GAIN}\geqslant g\left(\rho_0\right),\end{cases}$$

$$\Pi_{sum}=\begin{cases}M_L N_{fd}\left[4N_s+9N_s\log_2\left(N_s\right)+\left(1+1/M_L\right)N_c\right], & \\ & V_{GAIN}<g\left(\rho_0\right),\\ N_{fd}\left[4N_s+9N_s\log_2\left(N_s\right)+2N_c\right], & V_{GAIN}\geqslant g\left(\rho_0\right).\end{cases} \tag{22}$$

As Table 1 shows, the computational loads are in proportion to M; therefore, it can be denoted as $O(M)$. Diminishing non-coherent accumulation times can reduce the computational loads, which implies a decreases in both power dissipation and single dwell time. Furthermore, a decrease in the single dwell time leads to a decrease in MAT, which agrees with the conclusion obtained in the previous subsection.

Additionally, implementation of the proposed algorithm will not incur any noticeable increase in FPGA resource utilization compared with the conventional algorithm. In practice, the acquisition scheme is designed for not only strong signals but also weak and moderate signals; therefore, implementation is designed according to the most complex situations, i.e., integration of every working mode. Implementation of the proposed algorithm remains almost the same as that of the conventional algorithm, only with an additional module to realize mode switching. Because CNR estimation derived from the AGC control voltage can be pre-calculated, both the detection threshold corresponding to the additional working mode and the threshold $g(\rho_0)$ controlling the mode switching, can be pre-calculated and prestored. Therefore, the implementation of this simple control logic will not greatly increase resource utilization or implementation complexity.

5 Numerical results

The performance of the proposed algorithm was evaluated via a series of Monte Carlo simulations, and the results are presented in this section. Here, the receiver operating characteristic (ROC) curves, MAT, and computational complexity are considered. Furthermore, the performance of the conventional algorithm is analyzed for comparison. Corresponding to the previous section, the parallel and hybrid search strategies were simulated; the serial search strategy was omitted owing to its extraordinarily high time consumption. The simulations were run with the parameters listed in Table 2. The number of bins in the code phase domain and that in the Doppler frequency domain were N_c= 1023 and N_{fd}=19, respectively.

5.1 ROC curves

First, to verify the conclusion drawn in Subsection 4.1, the ROC curves with M=M_L and M=1 obtained by theoretical calculation according to (14) and (15) are illustrated in Figure 3(a). Here, parallel search is taken as an example. In this figure, M=M_L corresponding to the conventional algorithm and the lower CNR mode of the proposed algorithm and M=1 corresponding to the higher CNR mode of the proposed algorithm are illustrated for comparison. The differences in detection probabilities are given in (b). The figure shows that in the meaningful region, i.e., CNR$\geqslant\rho_0$, all of the differences in detection probabilities between the conventional and proposed algorithms, which correspond to the solid line, are less than 10^{-10}. The fluctuations are caused by the approximate numerical calculation. Therefore, the results agree well with the conclusion that when CNR$\geqslant\rho_0$, the detection performance of the proposed algorithm is very close to that of conventional algorithm. In addition, as mentioned before, when CNR$<\rho_0$, the detection probabilities of the proposed algorithm are identical to those of the conventional algorithm because of the same configuration being in use.

Table 2 Simulation conditions

Parameter	Value	Unit
Sampling frequency	4.096	MHz
CNR range under observation	25–65	dBHz
Lower bound of CNR in practice	37	dBHz
Modulation	BPSK	–
PRN number of GPS C/A code	1	–
Code rate	1.023	Mcps
Code length	1023	chip
Integration period	1	ms
M_L	10	–
Uncertainty region of f_d	–9–+9	kHz
Search step of f_d	1	kHz
Uncertainty region of τ	1–1023	chip
Search step of τ	1	chip
Penalty factor K_p	50	–
$\{\rho_{th},\rho_0\}$	{46,53}	dBHz

Additionally, the ROC curves obtained by simulation and theoretical calculation are shown for comparison in Figure 4. Here, several typical P_{FA} values and a large range of CNR values are taken into consideration. As shown in this figure, the simulated results for all $\{P_D, P_{FA}\}$ pairs are below $\{5\times10^3, 1\times10^8\}$ trials and they all agree very well with the theoretical results obtained from (15) and (18). Therefore, the accuracy of the analytical expressions is verified. The ROC curves for parallel search in (a) appear identical to those for hybrid search in (b), because for low false-alarm probability, both $P_D^{(p)}(\gamma)$ and $P_D^{(h)}(\gamma)$ approximate to $\int_{\gamma}^{\infty} f_{H1}(M,x)dx$ [29]. In the legend of the figure, "Theo", "Sim", "Pro" and "Con" are abbreviations for theoretical,

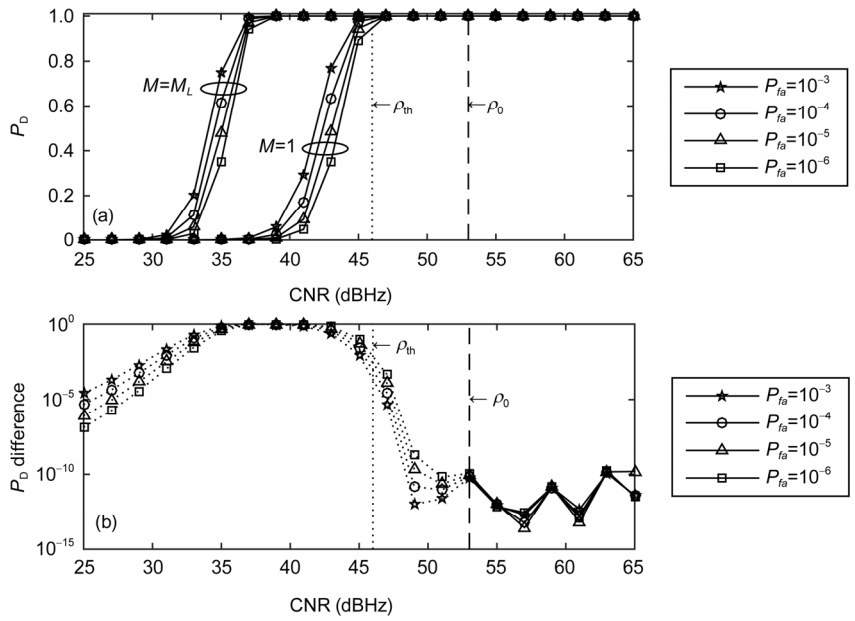

Figure 3 Theoretical differences in ROCs between conventional and proposed algorithms. (a) P_D curves; (b) P_D difference curves.

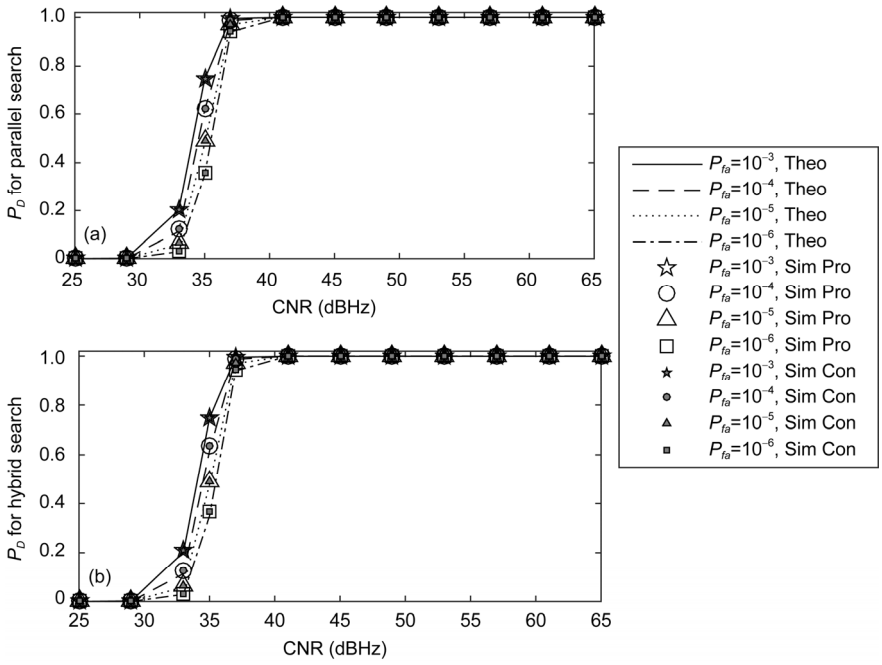

Figure 4 ROC curves of proposed and conventional algorithms obtained by theoretical calculation and simulations. (a) P_D for parallel search; (b) P_D for hybrid search.

simulated, proposed, and conventional, respectively.

5.2 MAT curves

Theoretical MAT curves for the conventional and proposed algorithms were obtained according to the equations derived in Subsection 4.2 and are illustrated in Figure 5. Figure 5(a) and (b) are MATs in units of T_{coh} for parallel search and (c) and (d) are MATs for hybrid search. Figure 5(a) and (c) are the MAT curves corresponding to a large range of CNR and (b) and (d) limit the CNR range to a smaller region of interest, i.e., CNR$\geqslant\rho_{th}$. Various false-alarm probability conditions are considered for hybrid search. When CNR$\geqslant\rho_{th}$, MATs of different false-alarm probability conditions show the same tendency and similar values. This result reveals that when CNR$\geqslant\rho_0$, the MAT of conventional algorithm is almost M_L times the MAT of proposed algorithm, which agrees with the analysis in Subsection 4.2. In addition, the

results validate the proposed algorithm from the perspective of time saving. The MAT in Figure 5(d) is almost five times that in (b), which agrees with that $T_{pro}^{(h)} \approx T_{pro}^{(p)} N / (2C_P)$ when $P_D^{(h)}(M,\gamma) \approx 1$ and $P_{FA}^{(h)}(M,\gamma) \approx 0$.

The simulation results of MAT are illustrated in Figure 6 to verify the theoretical values. For simplicity, only the proposed algorithm is analyzed here. The simulated curves coincide with the theoretical curves except in the region near ρ_0, where there is a slight deviation. The deviation arises because the relationship between the actual CNR and working mode is not deterministic with one-to-one mapping because of the estimation error of CNR introduced by AGC module around ρ_0. That is, small proportion of trials with CNR<ρ_0 work in the high CNR mode, i.e., M=1, and a small proportion of trials with CNR>ρ_0 work in the M=M_L mode. However, the simulation results can be concluded to be consistent with the theoretical results, because the slight

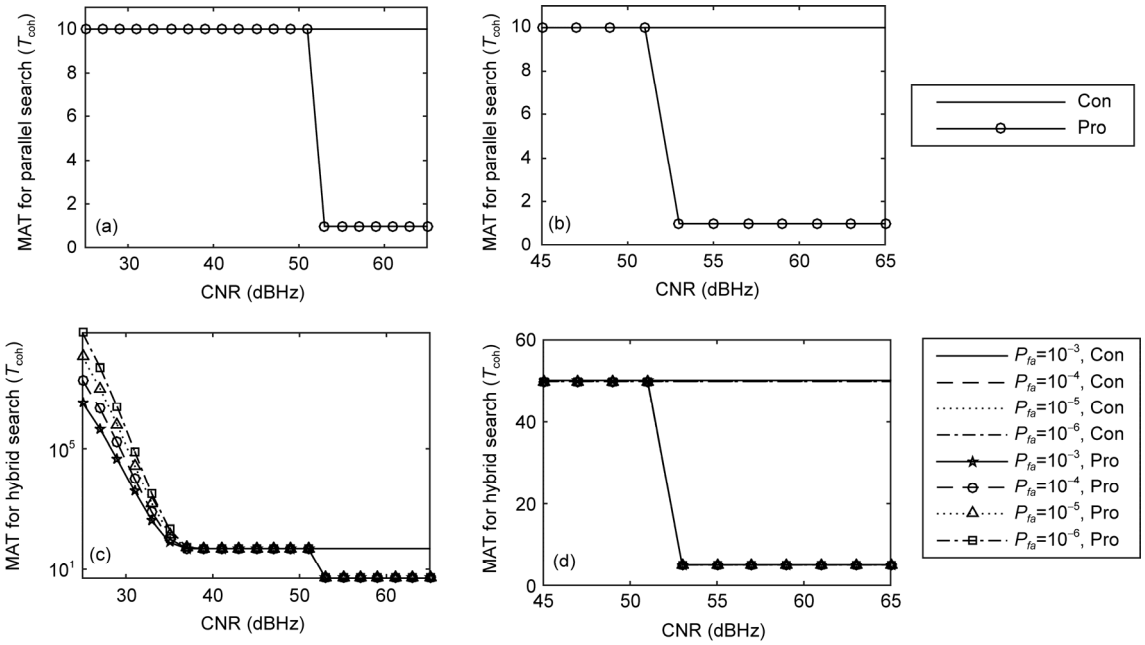

Figure 5 Theoretical MAT curves of conventional and proposed algorithms. (a) MAT for parallel search; (b) Partial MAT for parallel search; (c) MAT for hybrid search; (d) Partial MAT for hybrid search.

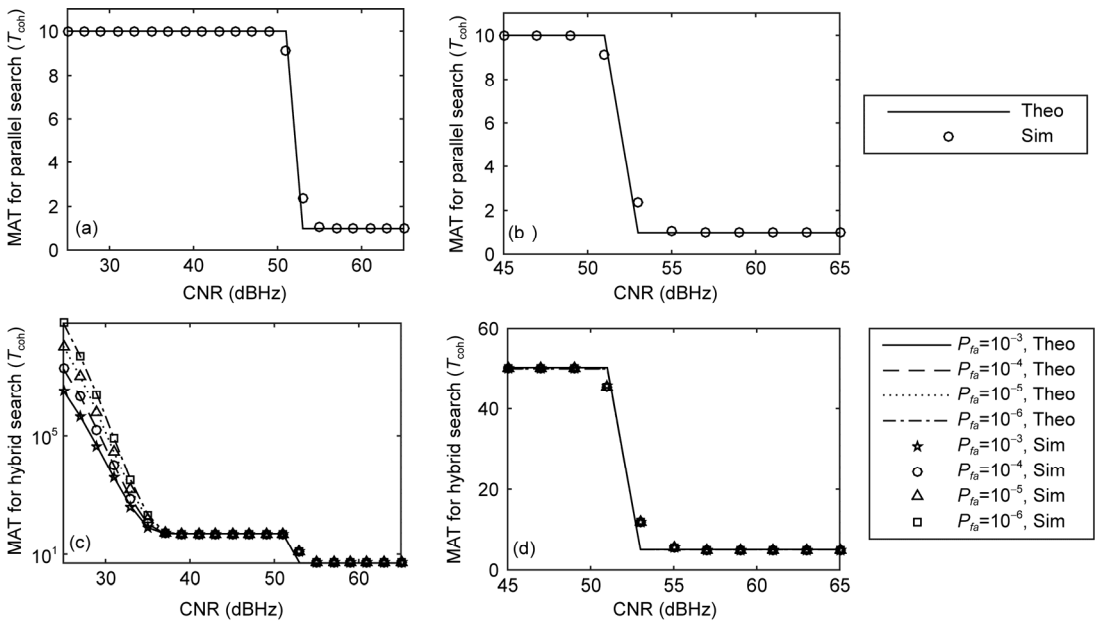

Figure 6 Theoretical and simulated MAT curves of the proposed algorithm. (a) MAT for parallel search; (b) Partial MAT for parallel search; (c) MAT for hybrid search; (d) Partial MAT for hybrid search.

deviation is simply present in a small region and is tolerable.

5.3 Computational complexity

By substituting the parameter set of M_L, N_c, N_{fd}, etc. into equation (22), the numerical results of computational load are listed in Table 3. The decrease in the computational load of the proposed algorithm for $V_{GAIN} \geqslant g(\rho_0)$ is proportional to M_L. This result means that, in practice, the proposed algorithm gives greater benefits in a larger dynamic range of signal power.

5.4 Performance at different code lengths

To verify the universality of the proposed algorithm for DSSS signals with different code lengths, the C/A code for the GLONASS system, whose code length is 511, was selected for simulations. The simulations were carried out at a sampling frequency of 2.048 MHz, a code rate of 511 kcps, a code length of 511 chips, an uncertainty region of code phase of 511 chips, and corresponding ρ_0=50 dBHz. The corresponding ROC and MAT curves are illustrated in Figure 7. Figure 7(a) shows that the proposed algorithm has a similar detection performance to the conventional algorithm and (b) demonstrates that the MAT of proposed algorithm is reduced greatly compared with the conventional algorithm when CNR$\geqslant\rho_0$. Therefore, the simulation results validate the proposed algorithm for a code length other than 1023 chips.

Table 3 Computational load

Type		Multiplication	Summation
Conventional		2.97×10^7	4.14×10^7
Proposed	$V_{GAIN} < g(\rho_0)$	2.97×10^7	4.14×10^7
	$V_{GAIN} \geqslant g(\rho_0)$	2.97×10^6	4.15×10^6

6 Conclusions

In this paper, an acquisition algorithm assisted by AGC control voltage has been proposed. The principles and procedures have been described in detail. The performance of the algorithm with respect to the detection and false-alarm probabilities, MAT, and computational load has been evaluated theoretically and verified by simulations. The results show that the proposed algorithm can reduce MAT especially in strong signal scenarios with neither obvious loss of detection performance nor increase in resources utilization. In addition, computational load and power dissipation are reduced within the effective CNR range. Because AGC is widely used in DSSS receivers, this algorithm is quite applicable in practice, and is extremely suitable for applications such as space-borne facilities owing to the good performance in power dissipation.

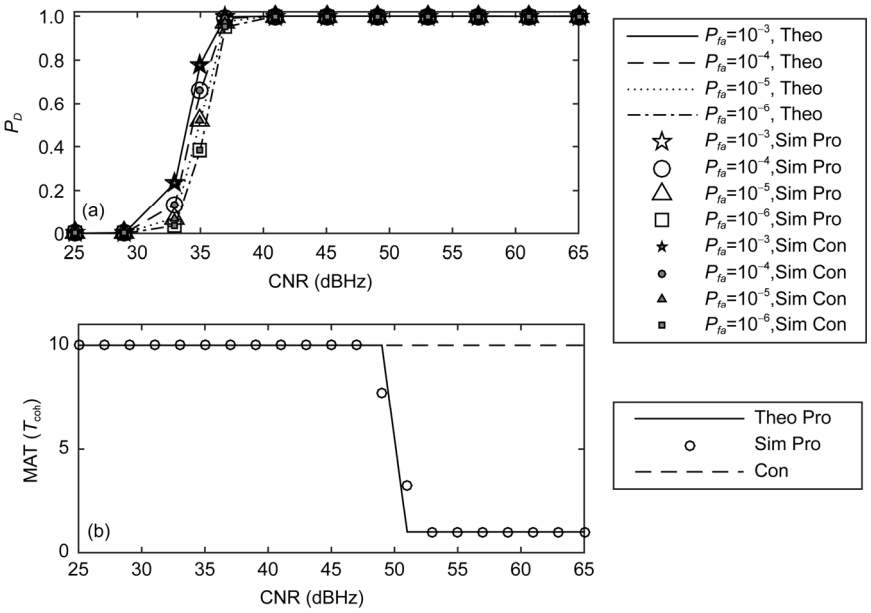

Figure 7 ROC and MAT curves of proposed algorithm for code length of 511. (a) P_D curves; (b) MAT curves.

This work was supported by the National Natural Science Foundation of China (Grant No.61401026) and the National High Technology Research and Development Program of China (Grant No.2014AA1070).

1 Zhang D H, Shi H, Jin Y Q, et al. The variation of the estimated GPS instrumental bias and its possible connection with ionospheric variability. Sci China Tech Sci, 2014, 57: 67–79

2 Shu F, You X H, Wang M, et al. Hybrid interference alignment and power allocation for multi-user interference MIMO channels. Sci China Inf Sci, 2013, 56: 042302

3 Wang J B, Chen M, Wang J Y, et al. Adaptive BER-constraint-based

power allocation for downlink MC-CDMA systems with linear MMSE receiver. Sci China Inf Sci, 2013, 56: 072305
4 Zheng J, Li J D, Shi H, et al. Joint subcarrier, code, and power allocation for parallel multi-radio access in heterogeneous wireless networks. Sci China Inf Sci, 2014, 57: 089301
5 Huang K W, Tao R, Wu K, et al. Study on interference suppression based on joint fractional Fourier domain and time domain. Sci China Tech Sci, 2011, 54: 2674–2686
6 Wang Y Q, Li C, Xu D, et al. A new barycenter code discriminator for multi-access interference. Sci China Inf Sci, 2014, 57: 022311
7 Arribas J, Fernandez-Prades C, Closas P. Antenna array based GNSS signal acquisition for interference mitigation. IEEE Trans Aerosp Electron Syst, 2013, 49: 223–243
8 Luo Y, Wang Y Q, Wu S L, et al. Multipath effects on vector tracking algorithm for GNSS signal. Sci China Inf Sci, 2014, 57: 102312
9 Luo Y, Wu W Q, Babu R, et al. A double-filter-structure based COMPASS/INS deep integrated navigation system implementation and tracking performance evaluation. Sci China Inf Sci, 2014, 57: 012206
10 Wang Y L, Liu W J, Xie W C, et al. Reduced-rank space-time adaptive detection for airborne radar. Sci China Inf Sci, 2014, 57: 082310
11 Zeng K, Peng Q H, Tang Y X. Mitigating spectrum sensing data falsification attacks in hard-decision combining cooperative spectrum sensing. Sci China Inf Sci, 2014, 57: 042318
12 Tian J, Cui W, Shen Q, et al. High-speed maneuvering target detection approach based on joint RFT and keystone transform. Sci China Inf Sci, 2013, 56: 062309
13 Leclere, J, Botteron C, Farine P A. Acquisition of modern GNSS signals using a modified parallel code-phase search architecture. Signal Process, 2014, 95: 177–191
14 Sagiraju, P K, Raju G V S, Akopian D. Fast acquisition implementation for high sensitivity global positioning systems receivers based on joint and reduced space search. IET on Radar, Sonar & Navigation, 2008, 2: 376–387
15 Iinatti, J H J. On the threshold setting principles in code acquisition of DS-SS signals. IEEE J Select Areas Commun, 2000, 18: 62–72
16 Sharawi M S, Akos D M, Aloi D N. GPS C/N0 estimation in the presence of interference and limited quantization levels. IEEE Trans Aerosp Electron Syst, 2007, 43: 227–238
17 Yeom S, Jung Y, Lee S. An adaptive threshold technique for fast PN code acquisition in DS-SS systems. IEEE Trans Veh Technol, 2011, 60: 2870–2875
18 Xu Y, Chang Q, Yu Z J. On new measurement and communication techniques of GNSS inter-satellite links. Sci China Tech Sci, 2012, 55: 285–294
19 O'Mahony N, Murphy C C, Lachapelle G. A dual-threshold up-down counter for GPS acquisition. Signal Process, 2011, 91: 1093–1102
20 Bastide F, Akos D, Macabiau C, et al. Automatic gain control (AGC) as an interference assessment tool. In: Proceedings of the 16th International Technical Meeting of the Satellite Division of The Institute of Navigation (ION GPS/GNSS 2003), 2001. 2042–2053
21 Akos, D M. Who's afraid of the spoofer? GPS/GNSS spoofing detection via automatic gain control (AGC). Navigation, 2012, 59: 281–290
22 Jafarnia A. GNSS signal authenticity verification in the presence of structural interference. Dissertation for the Doctoral Degree. Alberta: University of Calgary, 2013
23 Comparini M C, Tiberis F D E, Novello R, et al. Advances in deep-space transponder technology. Proceedings of the IEEE, 2007, 95: 1994–2008
24 Jayaram C, Murthy C R. Noncoherent integration for signal detection: analysis under model uncertainties. IEEE Trans Aerosp Electron Syst, 2013, 49: 2413–2430
25 Borio D, Akos D. Noncoherent integrations for GNSS detection: analysis and comparisons. IEEE Trans Aerosp Electron Syst, 2009, 45: 360–375
26 Shen Y Y, Wang Y Q, Chen J Y, et al. High sensitivity acquisition algorithm for DSSS signal with data modulation. China Commun, 2015, 12: 76–85
27 Analog Devices Inc. DataSheet-AD8367 500 m VGA with AGC detector. 2001
28 Yu X B, Chen X M, Bi G G, et al. Performance of orthogonal STBC-MIMO with variable power adaptive modulation and delayed feedback in Nakagami fading channels. Sci China Inf Sci, 2013, 56: 102308
29 Borio D. A statistical theory for GNSS signal acquisition. Dissertation for the Doctoral Degree. Torino: Politecnico Di Torino, 2008
30 Chugg K M, Zhu M R. A new approach to rapid PN code acquisition using iterative message passing techniques. IEEE J Select Areas Commun, 2005, 23: 884–897
31 Leclere J, Botteron C, Farine P A. Comparison framework of FPGA-based GNSS signals acquisition architectures. IEEE Trans Aerosp Electron Syst, 2013, 49: 1497–1518

Appendix A

To analyze the mutual relationship between the CNR of received signal and the AGC control voltage by using a numerical approach, an AD8367 AGC chip, manufactured by Analog Devices corporation, is cited an example. The control voltage V_{GAIN} can be derived from the equation given by the datasheet [27], which is

$$V_{IN-RMS}\,(\text{dBV rms}) = -54.02 + 50V_{GAIN}, \tag{A1}$$

where $V_{IN\text{-}RMS}$ is the root-mean-square (rms) voltage of the received signal. The received signal can be calculated by $P = V_{IN-RMS}^2 / R$, where R represents the input resistance of AGC signal power detector module.

Therefore, the expressions of η and V_{GAIN} can be rewritten as

$$\begin{cases} \eta = 10\log_{10}\dfrac{P_s}{P_n} = 10\log_{10}\left[\dfrac{10^{(-108.04+100V_{GAIN})/10}}{(\mathcal{K}TB)R} - 1\right], \\ V_{GAIN} = \dfrac{1}{100}\left\{108.04 + 10\log_{10}\left[\left(10^{\eta/10}+1\right)(\mathcal{K}TB)R\right]\right\} \\ \quad = \dfrac{1}{100}\left\{108.04 + 10\log_{10}\left(10^{\eta/10}+1\right) + 10\log_{10}R + P_n(\text{dB})\right\}. \end{cases} \tag{A2}$$

In addition, the CNR of received signal ρ can be calculated by η according to

$$\rho = \eta + 10\log_{10} B. \tag{A3}$$

Thus, the relationship between CNR and V_{GAIN}, which lays the foundation of the proposed algorithm, is illustrated in Figure A1.

Here, shorter codes with lengths of 255 and 511 are plotted, accompanied by the typical code length of 1023 for

comparison. As shown in Figure A1, when $\rho<\rho_0$, V_{GAIN} is insensitive to the CNR variation. This tendency agrees with the inherent property of DSSS signals that the desired signal power is overwhelmed by noise and occupies a tiny proportions in the combined signal power and its increase cannot effect a visible increase in V_{GAIN} in such situations. On the other hand, when $\rho>\rho_0$ such as in near-field receiver applications, the sensitivity of V_{GAIN} to the CNR variation increases. Therefore, a more accurate CNR estimation can be obtained with the assistance of AGC control voltage in high CNR scenarios. This imposes restrictions on the operating space of the proposed algorithm, i.e. $\rho>\rho_0$.

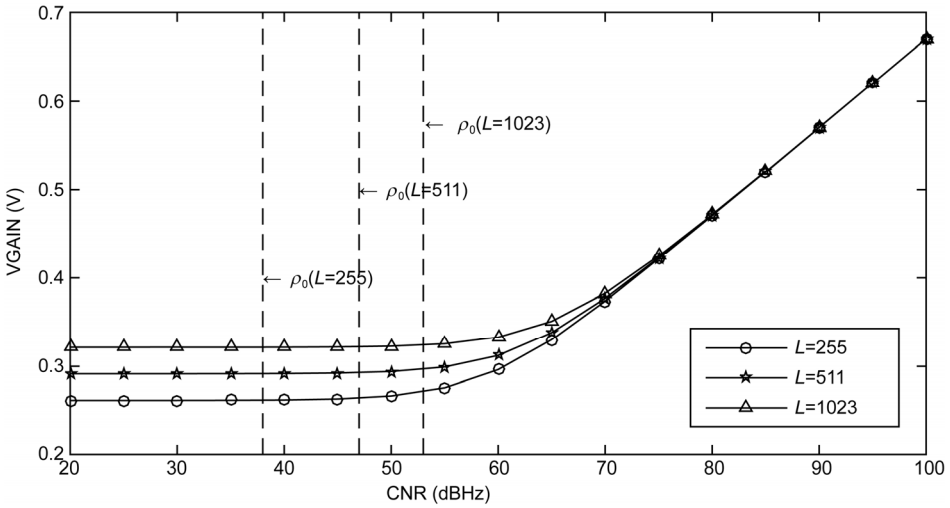

Figure A1 AGC control voltage versus CNR.